
Analytical model for low-frequency transmission loss calculation of membranes loaded with arbitrarily shaped masses

F. Langfeldt^a, W. Gleine^a, O. von Estorff^b

^a*Department of Automotive and Aeronautical Engineering, Hamburg University of Applied Sciences, Berliner Tor 9, D-20099 Hamburg, Germany*

^b*Institute of Modelling and Computation, Hamburg University of Technology, Denickestr. 17, D-21073 Hamburg, Germany*

Abstract

An analytical model for the transmission loss calculation of thin rectangular and circular membranes loaded with rigid masses of arbitrary shape, so-called membrane-type acoustic metamaterials, is presented. The coupling between the membrane and the added masses is introduced by approximating the continuous interaction force with a set of discrete point forces. This results in a generalized linear eigenvalue problem that is solved for the eigenfrequencies and eigenvectors of the coupled system. The concept of the effective surface mass density is employed to calculate the low-frequency transmission loss using the obtained eigenpairs. The proposed model is verified using numerical data from a finite element model and the convergence behavior of the point matching approach is investigated using Richardson extrapolation. Finally, a method based upon the grid convergence index for estimating the error that is introduced due to the point matching approach is presented.

Keywords: metamaterial, membrane, transmission loss, analytical model

*Corresponding author

Email address: Felix.Langfeldt@haw-hamburg.de (F. Langfeldt)

Post-print submitted to Journal of Sound and Vibration

February 11, 2015

©2015. This manuscript version is made available under the CC-BY-NC-ND 4.0 license.
<http://creativecommons.org/licenses/by-nc-nd/4.0/>

Please cite as: Langfeldt, F., Gleine, W. and O. von Estorff. Analytical model for low-frequency transmission loss calculation of membranes loaded with arbitrarily shaped masses. *Journal of Sound and Vibration* 349 (2015): 315–329.
<https://doi.org/10.1016/j.jsv.2015.03.037>

1. Introduction

In recent years, so-called membrane-type acoustic metamaterials (MAM) have emerged as a promising measure for attenuating sound propagation, especially in the low-frequency regime [1]. The name “acoustic metamaterial” describes structures which exhibit unusual mechanical properties, such as a negative mass and/or a negative bulk modulus, at wavelengths much greater than the size of the structure itself. Many different kinds of acoustic metamaterials, such as three-dimensional sonic crystals [2, 3] or one-dimensional resonator arrays [4, 5, 6], have been proposed recently. The membrane-type acoustic metamaterials distinguish themselves from other realisations of acoustic metamaterials by a very compact two-dimensional structure, where a thin membrane is loaded with one or more small masses. Such a lightweight arrangement is specifically applicable to engineering fields, where weight and installation space of sound attenuation means are highly constrained, e.g. in aeronautics. Experimental and numerical investigations of MAMs showed that in a certain frequency band the sound transmission loss of such a mass loaded membrane can exceed the corresponding mass law by far, showing a distinct peak at a specific frequency [1, 7]. This transmission loss peak frequency is controlled by the membrane design and, for fixed geometry, is mainly influenced by the magnitude of the added mass and the pretension of the membrane [1, 8, 9]. Further studies of MAMs showed that the stopping bandwidth of the metamaterial can be increased, e.g. by introducing additional transmission loss peaks using off-centered or multiple mass placement [7, 9] or by stacking multiple layers of MAMs with different transmission properties [7, 10]. Finally, additional investigations on the absorption behavior of MAMs showed that membrane-type metamaterials can also be applied as absorbent materials with nearly total absorption in the low frequency regime [11, 12].

In view of the high potential of MAMs in low frequency sound insulation, there is a demand for suitable and efficient models to estimate the transmission loss of MAMs a-priori, before first experimental prototypes are built. Numer-

ical methods, such as the finite element method (FEM), are the most general approach and have widely been used in the literature for the analysis of MAMs. These methods, however, can be quite cumbersome in automated design-processes (such as optimisations), since numerical grids are needed for
35 the membranes and the adjacent fluid and these grids have to be updated for every change in geometry (e.g. mass position). Therefore, analytical methods are a promising alternative for the transmission loss prediction of MAMs.

Some of the first theoretical studies of membranes loaded with a rigid mass were performed by Kornhauser and Mintzer [13] and Cohen and Handelman
40 [14], where the influence of a concentric circular mass on the natural frequencies of a circular membrane has been investigated. This case was further analyzed theoretically in [15], where natural frequencies and mode shapes are given for the concentrically loaded circular membrane. An analytical model of a mass loaded membrane specifically tailored for the application to MAMs was proposed by
45 Zhang et al. [9], where the Galerkin method is employed to obtain the forced vibration behavior of a rectangular membrane loaded with a rectangular mass. Later, Tian et al. [16] used the same approach to derive an analogous model for a circular membrane with a concentric ring mass. These two models, however, do not account for the rigidity and rotary inertia of the masses, which becomes
50 important for added masses of reasonable size, as shown in [15].

The most comprehensive analytical model of MAMs has recently been proposed by Chen et al. [17]. In this model, the point matching approach is employed at the interface boundary between the added masses and the membrane to account for the rigidity and the inertia of the masses. This results in a non-
55 linear eigenvalue problem which, once solved, delivers the natural frequencies and mode shapes of the loaded membrane. Then, the normal incidence transmission loss is calculated with the resulting membrane modes by solving the acoustic wave equation. While the analytical model proposed by Chen et al. [17] is the most universal one which allows for the analysis of membranes with
60 multiple masses of arbitrary shape at arbitrarily high frequencies, there are two challenging tasks within their model that impact the computational speed of

this method considerably: First, a non-linear eigenvalue problem needs to be solved in order to obtain the membrane eigenmodes, which requires an efficient root searching algorithm. Second, the normal incidence transmission loss is calculated by numerically integrating the Green's function of the acoustic wave equation across the membrane surface for each frequency. Both tasks require a large number of evaluations of the fundamental solutions of the membrane which can be a very time-consuming task, especially in the case of a circular membrane, where Bessel functions have to be evaluated.

The analytical model presented in this contribution overcomes these two issues to yield low-frequency transmission loss predictions of MAMs under normal sound incidence with the accuracy of the model by Chen et al. [17] and the computational efficiency of the models by Zhang et al. [9] and Tian et al. [16]. This is achieved by following the point matching approach of Chen et al. [17] to take into account the coupling between the membrane and the added mass(es) in a different way: First, instead of the introduction of matching points at the membrane-mass boundary only, the full membrane-mass coupling surface is covered with matching points. Second, the membrane displacement is expanded in the eigensolutions of the unloaded membrane, instead of solving the inhomogeneous Helmholtz-equation for the matching point forces directly. Thus, a linear eigenvalue problem for the modal participation factors and matching point forces (instead of a non-linear eigenvalue problem for the matching point forces only) is obtained. Additionally, a low-frequency approximation for the transmission loss that employs the effective surface mass density of the membrane allows the calculation of the MAM normal incidence transmission loss without numerical integration.

The present contribution is structured as follows: First, the analytical model is derived for rectangular as well as circular membrane geometries with a detailed explanation of the resulting eigenvalue problem and the normal incidence transmission loss calculation. Then, the model is verified for the two membrane geometries and different mass configurations with a finite element model and a discussion of the convergence behavior of the employed point matching approach

is given.

2. Analytical model

95 In this section, the analytical model is derived for the two most common membrane geometries: Rectangular and circular membranes. The model can be extended to different membrane shapes (e.g. triangular or polygonal membranes), as long as the fundamental mode shapes of these membrane geometries are known.

100 In the following sub-sections it is shown how to obtain the natural frequencies and mode shapes of a mass loaded rectangular membrane using the point matching approach. This is followed by the analysis of the circular membrane to show the similarities and differences between these geometries. Then it is described, how to calculate the low-frequency normal incidence transmission loss for both membrane geometries using the obtained natural frequencies and mode shapes. Finally, a brief explanation is given on how to obtain the transmission loss peak frequencies from the natural frequencies and mode shapes of the mass-loaded membrane.

2.1. Rectangular membrane

110 A rectangular membrane with edge lengths L_x and L_y , as shown in Fig. 1, is considered. A cartesian coordinate system is defined with the origin placed in one corner of the membrane, the x -axis pointing in L_x -direction, the y -axis pointing in L_y -direction, and the z -axis being perpendicular to the membrane surface. The membrane, with surface mass density m_m'' , is fixed along the edges and initially stressed by a uniform tension force per unit length T . A harmonic time dependence of the transverse vibrations with $w(x, y, t) = \hat{w}(x, y)e^{i\omega t}$ is assumed, where \hat{w} is the transverse vibration amplitude, $i = \sqrt{-1}$, and ω is the angular frequency. Thus, the membrane motion is governed by the inhomogeneous Helmholtz equation [18]

$$-m_m''\omega^2\hat{w} - T\nabla^2\hat{w} = \hat{P} + \hat{f}_M'' \quad (1)$$

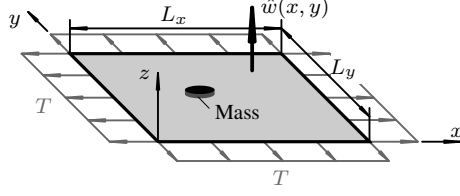


Figure 1: Definitions for the rectangular membrane configuration.

120 where $\nabla^2 = \partial^2/\partial x^2 + \partial^2/\partial y^2$ is the Laplace operator in cartesian coordinates and \hat{f}_M'' is the interface surface force amplitude between the membrane and the added masses. Since only normally incident plane acoustic waves are considered in the current model, the pressure amplitude \hat{P} is constant over the surface of the membrane. To turn Eq. (1) into a non-dimensionalized form, the following
 125 dimensionless quantities are introduced: The dimensionless coordinates $\xi = x/L_x$, $\eta = y/L_y$, and $\zeta = z/L_x$, the dimensionless membrane displacement amplitude $u = \hat{w}/L_x$, the aspect ratio $\Lambda = L_x/L_y$, the dimensionless frequency $k^2 = (m_m''/T)\omega^2 L_x^2$, the dimensionless pressure amplitude $\beta = \hat{P}L_x/T$, and the dimensionless interface surface force amplitude $\gamma'' = \hat{f}_M''/(TL_x)$. Thus, Eq. (1)
 130 turns into

$$-k^2 u - u_{\xi\xi} - \Lambda^2 u_{\eta\eta} = \beta + \gamma'', \quad (2)$$

where $u_{\xi\xi}$ and $u_{\eta\eta}$ refer to the second derivative of u with respect to ξ and η , respectively. The resulting boundary conditions for Eq. (2) are $u(0, \eta) = u(1, \eta) = u(\xi, 0) = u(\xi, 1) = 0$.

In general, the interface surface force amplitude γ'' is an unknown function
 135 of the membrane coordinates ξ and η . Therefore, the membrane-mass coupling is simplified with the point matching approach by approximating the continuous surface force amplitude γ'' by a set of point forces γ_i for each mass (see Fig. 2):

$$\gamma'' \approx \sum_{j=1}^{n_M} \sum_{i=1}^{I_j} \gamma_{ji} \delta(\xi - \xi_{ji}) \delta(\eta - \eta_{ji}) = \sum_{i=1}^I \gamma_i \delta(\xi - \xi_i) \delta(\eta - \eta_i), \quad (3)$$

where n_M is the number of added masses, I_j is the number of matching points
 140 for the j -th mass, $I = \sum_{j=1}^{n_M} I_j$ is the overall number of matching points, ξ_i and

η_i are the coordinates of the i -th matching point in the membrane coordinate system, and δ is the Dirac delta function. This changes the right hand side of the Helmholtz equation (2) into

$$-k^2 u - u_{\xi\xi} - \Lambda^2 u_{\eta\eta} = \beta + \sum_{i=1}^I \gamma_i \delta(\xi - \xi_i) \delta(\eta - \eta_i). \quad (4)$$

In order to find a solution of Eq. (4) for the membrane displacement amplitude u , the modal expansion technique is adopted: u is approximated by a finite linear combination of the membrane eigenfunctions $\Phi(\xi, \eta)$, which, in case of the rectangular membrane, are given by the product of two sine functions [18]:

$$u \approx \sum_{n=1}^N q_n \Phi_n = \sum_{n_x=1}^{N_x} \sum_{n_y=1}^{N_y} q_{n_x n_y} \sin(n_x \pi \xi) \sin(n_y \pi \eta), \quad (5)$$

where $N = N_x N_y$, $q_n = q_{n_x n_y}$, and $n = N_y(n_x - 1) + n_y$ is the running index variable. This expression is inserted into Eq. (4) which then is multiplied by an arbitrary eigenfunction Φ_m and integrated over the membrane surface to yield the following system of equations:

$$\sum_{n=1}^N (c_{mn} - k^2 m_{mn}) q_n = \beta b_m + \sum_{i=1}^I l_{mi} \gamma_i \quad (6)$$

which can be written in a more compact form as

$$(\mathbf{C} - k^2 \mathbf{M}) \mathbf{q} = \beta \mathbf{b} + \mathbf{L} \boldsymbol{\gamma}, \quad (7)$$

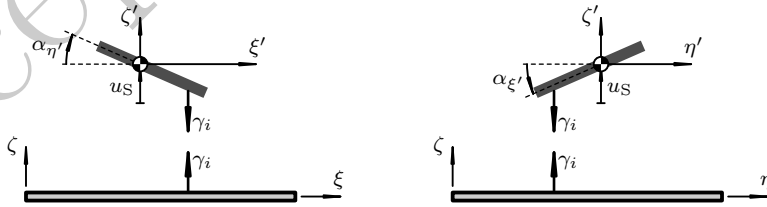


Figure 2: Illustration of the mass-membrane coupling using point forces and the resulting rigid body motion of the mass.

where the membrane stiffness matrix

$$\mathbf{C} = (c_{mn}) \in \mathbb{R}^{N \times N}, \quad c_{mn} = \begin{cases} \frac{\pi^2}{4} (n_x^2 + \Lambda^2 n_y^2) & \text{if } m = n \\ 0 & \text{else,} \end{cases} \quad (8)$$

155 and the membrane mass matrix

$$\mathbf{M} = (m_{mn}) \in \mathbb{R}^{N \times N}, \quad m_{mn} = \begin{cases} \frac{1}{4} & \text{if } m = n \\ 0 & \text{else,} \end{cases} \quad (9)$$

are both diagonal. The coupling matrix

$$\mathbf{L} = (l_{mi}) \in \mathbb{R}^{N \times I}, \quad l_{mi} = \sin(m_x \pi \xi_i) \sin(m_y \pi \eta_i), \quad (10)$$

is a fully populated rectangular matrix and the membrane excitation vector $\mathbf{b} \in \mathbb{R}^N$ is given by

$$\mathbf{b} = (b_n), \quad b_n = \begin{cases} \frac{4}{\pi^2 n_x n_y} & \text{if } n_x n_y \text{ odd} \\ 0 & \text{else.} \end{cases} \quad (11)$$

The coupling point force vector $\boldsymbol{\gamma} \in \mathbb{R}^I$ in Eq. (7) is unknown and needs to
 160 be determined before the system of equations can be solved for the membrane
 mode participation factors $\mathbf{q} \in \mathbb{R}^N$. To obtain an expression for $\boldsymbol{\gamma}$, the dynamic
 motion of the attached rigid masses, as shown in Fig. 2, needs to be analyzed.
 For this purpose, a local cartesian coordinate system $(\xi'_j, \eta'_j, \zeta'_j)$, with the origin
 located at the centre of gravity of the added mass, is introduced for each mass
 165 j (see Fig. 3). Due to the interaction between the membrane and the added
 mass j , the center of gravity of the mass displaces by $u_S^{(j)}$ and the mass rotates
 about the ξ'_j - and η'_j -axes by the angles $\alpha_{\xi'_j}^{(j)}$ and $\alpha_{\eta'_j}^{(j)}$, respectively (see Fig. 2).
 Hence, the kinematic displacement relationship of the mass j in terms of the
 local coordinate system is

$$u_M^{(j)} = u_S^{(j)} - \alpha_{\xi'_j}^{(j)} \xi'_j + \frac{1}{\Lambda} \alpha_{\eta'_j}^{(j)} \eta'_j. \quad (12)$$

170 The displacement $u_S^{(j)}$ and the rotations $\alpha_{\xi'_j}^{(j)}$ and $\alpha_{\eta'_j}^{(j)}$ are determined by applying
 Newton's second law to the translational motion of the mass in ζ'_j -direction

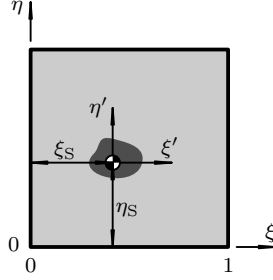


Figure 3: Definition of local mass coordinate system.

and Euler's equations to the angular motion of the mass about the ξ'_j - and η'_j -axes. With the mass ratio $\mu_j = M_j/(m''_m L_x^2)$, the dimensionless radii of gyration $\vartheta_{\xi'_j,j} = J_{x'_j,j}/(M_j L_x^2)$ and $\vartheta_{\eta'_j,j} = J_{y'_j,j}/(M_j L_x^2)$, where M_j is the j -th
 175 added mass magnitude and $J_{x'_j,j}$ and $J_{y'_j,j}$ are the moments of inertia of the j -th mass about the local x'_j - and y'_j -axes, respectively, the dimensionless equations of motion for each rigid mass j are:

$$u_S^{(j)} = \frac{1}{\mu_j k^2} \sum_{i=1}^{I_j} \gamma_{ji}, \quad (13a)$$

$$\alpha_{\xi'}^{(j)} = \frac{1}{\mu_j k^2} \frac{1}{\Lambda \vartheta_{\xi'_j,j}} \sum_{i=1}^{I_j} \eta'_{ji} \gamma_{ji}, \text{ and} \quad (13b)$$

$$\alpha_{\eta'}^{(j)} = -\frac{1}{\mu_j k^2} \frac{1}{\vartheta_{\eta'_j,j}} \sum_{i=1}^{I_j} \xi'_{ji} \gamma_{ji}. \quad (13c)$$

These equations are substituted into Eq. (12), which yields

$$u_M^{(j)} = \frac{1}{\mu_j k^2} \sum_{i=1}^{I_j} \left(1 + \frac{\xi'_j \xi'_{ji}}{\vartheta_{\eta'_j,j}} + \frac{\eta'_j \eta'_{ji}}{\Lambda^2 \vartheta_{\xi'_j,j}} \right) \gamma_{ji}. \quad (14)$$

180 Finally, the motion of each mass j is coupled to the membrane motion by enforcing the continuity of displacement amplitudes at each matching point location:

$$u_M^{(j)}(\xi'_{jm}, \eta'_{jm}) \stackrel{!}{=} u(\xi_{jm}, \eta_{jm}), \quad 1 \leq j \leq n_M, \quad 1 \leq m \leq I_j. \quad (15)$$

With Eqs. (5) and (14), this can be written in a more compact form as

$$-\mathbf{L}^T \mathbf{q} + \frac{1}{k^2} \mathbf{G} \boldsymbol{\gamma} = \mathbf{0}, \quad (16)$$

where

$$\mathbf{G} = \begin{bmatrix} \frac{1}{\mu_1} \mathbf{G}_1 & & \mathbf{0} \\ & \ddots & \\ \mathbf{0} & & \frac{1}{\mu_{n_M}} \mathbf{G}_{n_M} \end{bmatrix} \in \mathbb{R}^{I \times I} \quad (17)$$

and $\mathbf{G}_j = (g_{mn}^{(j)}) \in \mathbb{R}^{I_j \times I_j}$ are symmetric matrices with

$$g_{mn}^{(j)} = 1 + \frac{\xi'_{jm} \xi'_{jn}}{\vartheta_{\eta'_{j,j}}} + \frac{\eta'_{jm} \eta'_{jn}}{\Lambda^2 \vartheta_{\xi'_{j,j}}}. \quad (18)$$

185 It must be noted that the motion of a rigid mass is fully determined by the deflection amplitude of three non-collinear matching points, which means that the rank of the matrices \mathbf{G}_j cannot be greater than 3. Therefore, the matrix \mathbf{G} generally has rank $3n_M$ and thus is singular in most cases.

Equations (7) and (16) can now be combined to form the following system
190 of equations for the unknown vectors \mathbf{q} and $\boldsymbol{\gamma}$:

$$\begin{bmatrix} \mathbf{C} - k^2 \mathbf{M} & -\mathbf{L} \\ -\mathbf{L}^T & \frac{1}{k^2} \mathbf{G} \end{bmatrix} \begin{pmatrix} \mathbf{q} \\ \boldsymbol{\gamma} \end{pmatrix} = \beta \begin{pmatrix} \mathbf{b} \\ \mathbf{0} \end{pmatrix}. \quad (19)$$

The homogenous form of Eq. (19) can be rewritten as the generalized eigenvalue problem

$$\mathbf{A} \mathbf{x} = k^2 \mathbf{B} \mathbf{x}, \quad (20)$$

where

$$\mathbf{A} = \begin{bmatrix} \mathbf{C} & -\mathbf{L} \\ \mathbf{0} & \mathbf{G} \end{bmatrix}, \quad \mathbf{B} = \begin{bmatrix} \mathbf{M} & \mathbf{0} \\ \mathbf{L}^T & \mathbf{0} \end{bmatrix} \quad \text{and} \quad \mathbf{x} = \begin{pmatrix} \mathbf{x}_q \\ \mathbf{x}_\gamma \end{pmatrix}. \quad (21)$$

This eigenvalue problem can be solved for the mass-loaded membrane eigenvalues k_i^2 and the corresponding membrane mode eigenvectors $\mathbf{x}_q^{(i)}$ and mass
195 force eigenvectors $\mathbf{x}_\gamma^{(i)}$ with standard linear algebra methods. It is noteworthy that, in general, the matrices \mathbf{A} and \mathbf{B} are both singular, since \mathbf{G} is singular, as discussed above. Therefore, a suitable algorithm for the solution of the eigenvalue problem needs to be chosen. Furthermore, the algorithm should exploit
200 the sparsity of \mathbf{A} and \mathbf{B} for an efficient calculation of the eigenvalues. In the present investigations, the shift-and-invert technique is employed in order to transform the system (20) into a standard eigenvalue problem [19]. The shift φ

is selected so that the matrix $\mathbf{S} = \mathbf{A} - \varphi\mathbf{B}$ becomes regular and the eigenvalue problem (20) is transformed into

$$\mathbf{B}\mathbf{x} = \tilde{\varphi}\mathbf{S}\mathbf{x}, \quad (22)$$

205 with the transformed eigenvalues $\tilde{\varphi} = 1/(k^2 - \varphi)$. Eq. (22) can be reduced to standard form by left-multiplying with the inverse of \mathbf{S} . The resulting standard eigenvalue problem then is solved for the transformed eigenvalues $\tilde{\varphi}$ and eigenvectors \mathbf{x} using Arnoldi's method for sparse matrices [19]. During this procedure, the inverse of \mathbf{S} should not be calculated directly, in order not to give
210 up the sparseness of the problem.

2.2. Circular membrane

The analysis of the mass-loaded circular membrane can be conducted analogously to the rectangular membrane analysis. In fact, the forced response equation and the eigenvalue problem have the same structure as Eqs. (19) and
215 (20), respectively; only the matrices \mathbf{C} , \mathbf{M} , \mathbf{L} and \mathbf{G} as well as the vector \mathbf{b} are different. Therefore, in the following only these quantities will be derived for the circular case.

Fig. 4 shows the basic definitions of the circular membrane, with radius R , surface mass density m_m'' and uniform tension force per unit length T . A
220 cylindrical coordinate system, positioned in the center of the membrane with the radial and azimuthal coordinates r and θ , respectively, is used to describe the membrane displacement amplitudes \hat{w} in the Helmholtz equation (1). For the cylindrical coordinate system, the Laplace operator is given by $\nabla^2 = \partial^2/\partial r^2 +$

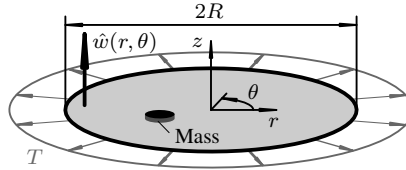


Figure 4: Definitions for the circular membrane configuration.

$1/r \partial/\partial r + 1/r^2 \partial^2/\partial \theta^2$. The following dimensionless quantities are introduced:

225 The dimensionless coordinates are $\xi = r/R$ and $\zeta = z/R$, the dimensionless membrane displacement amplitude is $u = \hat{w}/R$, the dimensionless frequency is $k^2 = (m_m''/T)\omega^2 R^2$, the dimensionless pressure amplitude is $\beta = \hat{P}R/T$, and the dimensionless mass coupling surface force amplitude is $\gamma'' = \hat{f}_M''/(TR)$. Substituting γ'' by a series of discrete point forces γ_i leads to the following

230 non-dimensional equation of motion for the circular membrane:

$$-k^2 u - \frac{1}{\xi} (\xi u_\xi)_\xi - \frac{1}{\xi^2} u_{\theta\theta} = \beta + \frac{1}{\xi} \sum_{i=1}^I \gamma_i \delta(\xi - \xi_i) \delta(\theta - \theta_i). \quad (23)$$

The boundary conditions for Eq. (23) are $u(1, \theta) = 0$ and $u(\xi, 2\pi + \theta) = u(\xi, \theta)$, which are fulfilled by the eigenfunctions [18]

$$\Phi_{n_\theta n_r} = J_{n_\theta}(\lambda_{n_\theta n_r} \xi) [\cos(n_\theta \theta) + C_{n_\theta n_r} \sin(n_\theta \theta)], \quad (24)$$

where J_{n_θ} is the n_θ -th order Bessel function of the first kind, $0 \leq n_\theta < N_\theta$, $\lambda_{n_\theta n_r}$ is the n_r -th root of J_{n_θ} , $1 \leq n_r \leq N_r$, and $C_{n_\theta n_r}$ is a constant. These

235 eigenfunctions are split up into cosine- and sine-parts

$$\Phi_{n_\theta n_r}^c = J_{n_\theta}(\lambda_{n_\theta n_r} \xi) \cos(n_\theta \theta) \quad \text{and} \quad (25a)$$

$$\Phi_{n_\theta n_r}^s = J_{n_\theta}(\lambda_{n_\theta n_r} \xi) \sin(n_\theta \theta) \quad (25b)$$

to yield the following modal expansion of u :

$$u \approx \sum_{n=1}^N q_n \Phi_n = \sum_{n_r=1}^{N_r} \sum_{n_\theta=0}^{N_\theta-1} q_{n_\theta n_r}^c \Phi_{n_\theta n_r}^c + \sum_{n_r=1}^{N_r} \sum_{n_\theta=1}^{N_\theta-1} q_{n_\theta n_r}^s \Phi_{n_\theta n_r}^s, \quad (26)$$

where the total number of considered eigenmodes is $N = 2N_r N_\theta - N_\theta$. For values of the running index n inside the range $1 \leq n \leq N_r N_\theta$, the modal participation factors q_n and eigenfunctions Φ_n correspond to the cosine-part in

240 Eq. (25a) with $n = N_\theta(n_r - 1) + n_\theta + 1$ ($0 \leq n_\theta < N_\theta$ and $1 \leq n_r \leq N_r$). For $N_r N_\theta < n \leq N$, on the other hand, q_n and Φ_n are assigned to the sine-part of the eigenfunctions in Eq. (25b) with $n = N_r N_\theta + N_\theta(n_r - 1) + n_\theta$ ($1 \leq n_\theta < N_\theta$ and $1 \leq n_r \leq N_r$). This is inserted into Eq. (23) which then is multiplied by an arbitrary eigenfunction Φ_m and integrated to yield the already known system

245 (7). For the circular membrane, however, the matrices \mathbf{C} , \mathbf{M} , and \mathbf{L} as well as the vector \mathbf{b} are different: The elements of the membrane stiffness matrix $\mathbf{C} = (c_{mn}) \in \mathbb{R}^{N \times N}$ are

$$c_{mn} = \begin{cases} \pi \lambda_{0n_r}^2 J_1(\lambda_{0n_r})^2 & \text{if } m = n \wedge n_\theta = 0 \\ -\frac{\pi}{2} \lambda_{n_\theta n_r}^2 J_{n_\theta-1}(\lambda_{n_\theta n_r}) J_{n_\theta+1}(\lambda_{n_\theta n_r}) & \text{if } m = n \wedge n_\theta > 0 \\ 0 & \text{else,} \end{cases} \quad (27)$$

the membrane mass matrix is $\mathbf{M} = (m_{mn}) \in \mathbb{R}^{N \times N}$, with

$$m_{mn} = \begin{cases} \pi J_1(\lambda_{0n_r})^2 & \text{if } m = n \wedge n_\theta = 0 \\ -\frac{\pi}{2} J_{n_\theta-1}(\lambda_{n_\theta n_r}) J_{n_\theta+1}(\lambda_{n_\theta n_r}) & \text{if } m = n \wedge n_\theta > 0 \\ 0 & \text{else,} \end{cases} \quad (28)$$

and the coupling matrix $\mathbf{L} = (l_{mi}) \in \mathbb{R}^{N \times I}$, with

$$l_{mi} = \begin{cases} J_{m_\theta}(\lambda_{m_\theta m_r} \xi_i) \cos(m_\theta \theta_i) & \text{if } m \leq N_r N_\theta \\ J_{m_\theta}(\lambda_{m_\theta m_r} \xi_i) \sin(m_\theta \theta_i) & \text{if } m > N_r N_\theta. \end{cases} \quad (29)$$

250 Finally, the membrane excitation vector $\mathbf{b} = (b_n) \in \mathbb{R}^N$ is given by

$$b_n = \begin{cases} \frac{2\pi}{\lambda_{0n_r}} J_1(\lambda_{0n_r}) & \text{if } n_\theta = 0 \\ 0 & \text{else.} \end{cases} \quad (30)$$

The derivation of the coupling relationship between the membrane modes and the coupling point force vector $\boldsymbol{\gamma}$ follows the same approach as in the rectangular membrane case. In fact, the same displacement continuity equation as Eq. (16) results, where, in this case however, the mass ratio μ_j is defined as
 255 $\mu_j = M_j / (m_m'' R^2)$ and the elements of $\mathbf{G}_j = (g_{mn}^{(j)}) \in \mathbb{R}^{I_j \times I_j}$ are given by

$$g_{mn}^{(j)} = 1 + \frac{\xi_{jm}' \xi_{jn}'}{\vartheta_{\eta_j', j}} + \frac{\eta_{jm}' \eta_{jn}'}{\vartheta_{\xi_j', j}}, \quad (31)$$

with the local cartesian mass coordinates $\xi_j' = x_j' / R$ and $\eta_j' = y_j' / R$, as well as the dimensionless radii of gyration $\vartheta_{\xi_j', j} = J_{x_j', j} / (M_j R^2)$ and $\vartheta_{\eta_j', j} = J_{y_j', j} / (M_j R^2)$.

Finally, the eigenvalues and eigenvectors of the mass-loaded circular membrane can be obtained, when the eigenvalue problem (20) is solved using the
 260 matrices \mathbf{C} , \mathbf{M} , \mathbf{L} , and \mathbf{G} derived above for the circular membrane case.

2.3. Low-frequency transmission loss

The eigenvalues and eigenvectors obtained by the solution of the eigenvalue problem presented above are used to calculate the normal incidence transmission loss of the membrane. Since MAMs are primarily applicable for the attenuation of low-frequency sound transmission, an approximate method to obtain the low-frequency normal incidence transmission loss is considered here.

At low frequencies with acoustic wavelengths greater than the characteristic dimension of a structure the sound radiation behavior of that structure is mainly governed by its surface-averaged vibration amplitude or piston-like motion [20]. Hence, the membrane can be regarded as a rigid wall with an effective surface mass density \tilde{m}'' at low enough frequencies. This effective surface mass density is defined as [1]

$$\tilde{m}'' = \frac{\langle \Delta \hat{P} \rangle}{\langle \hat{a}_z \rangle}, \quad (32)$$

where $\Delta \hat{P}$ is the pressure amplitude difference along the membrane surface, \hat{a}_z is the vibrational acceleration amplitude in normal direction of the membrane surface, and

$$\langle v \rangle = \frac{1}{S} \int_S v \, dS \quad (33)$$

denotes the surface average of a quantity v performed over the membrane surface S . Alternatively, a Green's function approach using the eigenmodes of the MAM can be used to obtain the effective surface mass density [21, 22]. Generally, \tilde{m}'' is frequency dependent and it can be used in accordance to the mass-law relationship to obtain the acoustic transmission factor

$$t = \frac{1}{1 + \frac{i\omega\tilde{m}''}{2\rho_0c_0}}, \quad (34)$$

where ρ_0 and c_0 are the density and speed of sound of the surrounding medium, respectively. Thus, the membrane sound transmission loss is given by $TL = -20 \log |t|$.

In order to obtain the effective surface mass density of a membrane at normal sound incidence, the pressure amplitude difference $\Delta \hat{P}$ in Eq. (32) can be

replaced by $\hat{P} = \text{const}$, without loss of generality. For harmonic vibrations, the acceleration amplitude is given by $\hat{a}_z = -\omega^2 \hat{w}$ and with the same non-dimensional parameters as above, the following expression for \tilde{m}'' results:

$$\tilde{m}'' = -m_m'' \frac{\beta}{k^2} \frac{1}{\langle u \rangle}. \quad (35)$$

According to the modal expansions of u in Eqs. (5) and (26), the surface averaged
 290 dimensionless displacement amplitude is given by

$$\langle u \rangle = \frac{1}{\sigma} \mathbf{b}^T \mathbf{q}, \quad (36)$$

where σ is the dimensionless membrane surface area which is $\sigma = 1$ for the rectangular membrane and $\sigma = \pi$ for the circular membrane. Since the eigenvectors $\mathbf{x}^{(i)}$ are obtained from solving the eigenvalue problem in Eq. (20), the membrane mode participation factors \mathbf{q} and the point mass vector $\boldsymbol{\gamma}$ can be expanded as a
 295 series of the corresponding parts of the eigenvectors $\mathbf{x}_q^{(i)}$ and $\mathbf{x}_\gamma(i)$, respectively, by defining

$$\mathbf{q} \approx \sum_{i=1}^K c_i \mathbf{x}_q^{(i)} = \mathbf{X}_q \mathbf{c} \quad \text{and} \quad \boldsymbol{\gamma} \approx \sum_{i=1}^K c_i \mathbf{x}_\gamma(i) = \mathbf{X}_\gamma \mathbf{c}, \quad (37)$$

where K is the number of eigenpairs obtained from Eq. (20) and c_i are the mode participation factors of the mass-loaded membrane. This is inserted into Eq. (19) and the participation factors for a mass-loaded membrane excited by a
 300 uniform pressure of amplitude β are obtained from the solution of the system

$$\left(\hat{\mathbf{A}} - k^2 \hat{\mathbf{B}} \right) \mathbf{c}^* = \hat{\mathbf{b}}, \quad (38)$$

where $\hat{\mathbf{A}} = \mathbf{X}^T \mathbf{A} \mathbf{X}$ and $\hat{\mathbf{B}} = \mathbf{X}^T \mathbf{B} \mathbf{X}$ are the reduced system matrices, $\hat{\mathbf{b}} = \mathbf{X}_q^T \mathbf{b}$, and $\mathbf{c}^* = \mathbf{c}/\beta$. Since \mathbf{X} is the matrix of linear independent generalized eigenvalues of (\mathbf{A}, \mathbf{B}) , this system of equations is further simplified by noting that $\mathbf{A} \mathbf{X} = \mathbf{B} \mathbf{X} \boldsymbol{\Lambda}$, where $\boldsymbol{\Lambda}$ is a diagonal matrix of the obtained mass-loaded
 305 membrane eigenvalues k_i^2 . Thus, $\hat{\mathbf{A}} = \hat{\mathbf{B}} \boldsymbol{\Lambda}$ and Eq. (38) simplifies to

$$\left(\boldsymbol{\Lambda} - k^2 \mathbf{I} \right) \mathbf{c}^* = \hat{\mathbf{a}}, \quad (39)$$

with the identity matrix \mathbf{I} and $\hat{\mathbf{a}} = \hat{\mathbf{B}}^{-1} \hat{\mathbf{b}}$.

With the definition of $\mathbf{q} \approx \mathbf{X}_q \mathbf{c}$, the surface averaged dimensionless displacement amplitude is expressed as

$$\langle u \rangle = \frac{1}{\sigma} \mathbf{b}^T \mathbf{X}_q \mathbf{c} = \frac{\beta}{\sigma} \hat{\mathbf{b}}^T \mathbf{c}^* \quad (40)$$

and the equation for the effective surface mass density (35) then results in

$$\tilde{m}'' = -\frac{m_m''}{k^2 \hat{\mathbf{b}}^T (\boldsymbol{\Lambda} - k^2 \mathbf{I})^{-1} \hat{\mathbf{a}}} \quad (41)$$

310 for the rectangular membrane and

$$\tilde{m}'' = -\frac{\pi m_m''}{k^2 \hat{\mathbf{b}}^T (\boldsymbol{\Lambda} - k^2 \mathbf{I})^{-1} \hat{\mathbf{a}}} \quad (42)$$

for the circular membrane.

Finally, it should be noted that the analytical model derived above is valid in the case of an undamped membrane structure. If structural damping of the membrane material needs to be considered, the membrane stiffness matrix \mathbf{C} 315 can be replaced by a complex stiffness matrix $\tilde{\mathbf{C}} = (1 + i\eta_m)\mathbf{C}$, where η_m is the structural loss factor of the membrane material.

2.4. Calculation of transmission loss peak frequencies

From the definition of the mass law transmission factor in Eq. (34) it can be seen that zero transmission of sound, i.e. $t \rightarrow 0$, occurs, if the magnitude of 320 the effective surface mass density of the membrane goes to infinity. This is the case, as evident from Eqs. (41) and (42), for non-zero frequencies k_P , when

$$\hat{\mathbf{b}}^T (\boldsymbol{\Lambda} - k_P^2 \mathbf{I})^{-1} \hat{\mathbf{a}} \stackrel{!}{=} 0. \quad (43)$$

Since the membrane eigenvalue matrix $\boldsymbol{\Lambda}$ is diagonal, this equation can be rewritten as a sum of partial fractions:

$$\sum_{i=1}^K \frac{A_i}{k_i^2 - k_P^2} \stackrel{!}{=} 0, \quad (44)$$

where the residuals are given by $A_i = \hat{b}_i \hat{a}_i$. Hence, the low-frequency transmission loss peak frequencies k_P of a mass-loaded membrane are obtained as the 325 roots of the rational function in Eq. (44).

3. Verification

To demonstrate that the analytical model is derived correctly, a verification of the model is performed by comparing the analytically predicted transmission loss of different membrane configurations to the results obtained by a finite element model. First, a detailed description of the finite element model is given in this section. Then, the analytical and numerical normal incidence transmission loss results are compared for a rectangular as well as circular membrane to verify the analytical model. Finally, a brief discussion on the convergence behavior of the coupling points is given and a method for estimating error bounds on the analytically predicted frequencies is presented.

3.1. Finite element model

The basic system to be modeled by finite elements is shown in Fig. 5, exemplarily for the case of a rectangular membrane. The model consists of a membrane with fixed edges and two prismatic acoustic cavities that are attached to each side of the membrane structure. The lateral surfaces of both cavities are defined as acoustically hard and the cavities are terminated by fully absorbing boundaries in order to simulate the conditions inside an impedance tube. The membrane is excited by a uniform harmonic pressure with amplitude $\hat{P} = 1$ Pa and the resulting transmitted acoustic pressure amplitude \hat{p}_t is obtained from

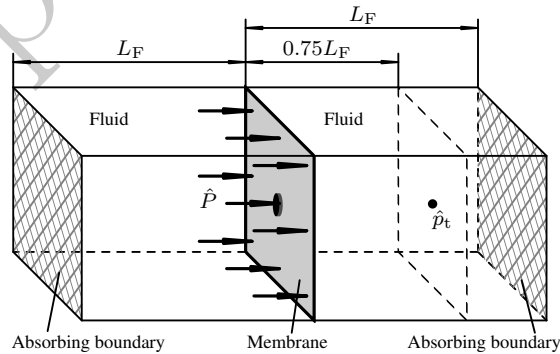


Figure 5: System modeled by finite elements for the verification of the analytical model.

a field point that is at a distance of three quarters of the cavity length from the membrane plane. Since only normally incident plane acoustic waves are generated by this approach, one field point is sufficient for the calculation of \hat{p}_t . The acoustic transmission factor is calculated as:

$$t = 2e^{0.75(i\omega L_F/c_0)} \frac{\hat{p}_t}{\hat{P}}. \quad (45)$$

350 For the discretization of the membrane, first order triangular elements with negligible bending and shear stiffness are used. The attached masses are modeled by volumetric elements and the fluid is discretized with first order tetrahedral fluid elements. The vibro-acoustic coupling is established via coincident grid nodes at the membrane-fluid interfaces. In order to obtain a proper pre-
355 stressing of the membrane material, a static temperature load is applied to the membrane elements before the dynamic analysis is performed. The necessary temperature load is obtained from [23]

$$\Delta\vartheta = -\frac{T}{Eh\alpha}, \quad (46)$$

where E is the membrane Young's modulus, h the membrane thickness, and α the thermal expansion coefficient of the membrane material. With this temper-
360 ature load a static analysis is performed and the results are used in conjunction with a linear perturbation method to obtain the direct frequency response of the pre-stressed membrane.

The verification of the analytical model is performed for the two geometrical cases (rectangular and circular) considered in the present contribution. In
365 both cases polyetherimid (PEI), with density $\rho = 1270 \text{ kg/m}^3$, Young's modulus $E = 2.9 \text{ GPa}$, and Poisson's ratio $\nu = 0.44$, is chosen to specify the membrane material. The membrane thickness is $h = 25 \text{ }\mu\text{m}$ which yields a membrane surface mass density of $m''_m = 31.75 \text{ g/m}^2$. Finally, the membrane pretension force per unit length is given by $T = 160 \text{ N/m}$. Without loss of generality, a unit thermal
370 expansion coefficient of $\alpha = 1 \text{ 1/K}$ is defined for the membrane which results in a static pre-loading temperature difference of $\Delta\vartheta = -2.207 \text{ mK}$. Circular added masses are chosen for the verification process, where the mass material

is steel, with $\rho_M = 7860 \text{ kg/m}^3$, $E_M = 210 \text{ GPa}$, and $\nu_M = 0.3$, and the mass radius is given by $R_M = 2 \text{ mm}$. The thickness of the steel disc is derived from
 375 the added mass magnitude $M = 0.2 \text{ g}$ according to $h_M = M/(\rho_M \pi R_M^2) \approx 2 \text{ mm}$. For the ambient fluid, standard atmospheric conditions of air are assumed with $\rho_0 = 1.225 \text{ kg/m}^3$ and $c_0 = 340 \text{ m/s}$ and the examined frequencies range from $f = 100$ to 1000 Hz .

3.2. Rectangular membrane

380 The rectangular membrane considered here is square with edge lengths $L_x = L_y = 20 \text{ mm}$ and the acoustic cavity length is chosen sufficiently large with $L_F = L_x$, such that the absorbing boundaries are outside the acoustical near field of the membrane. To obtain a grid-independent solution, the average element edge lengths of the membrane and the fluid are set to $\Delta_m = 0.5 \text{ mm}$ and $\Delta_f =$
 385 2.5 mm , respectively, after a grid-sensitivity analysis has been performed. In the analytical analysis, 160 membrane modes are considered in each spatial direction which yields a total number of membrane modes of $N = 25600$. $I = 228$ coupling points are evenly distributed across the membrane-mass interface area with an average matching point distance of $\Delta_\gamma = 0.25 \text{ mm}$. The first
 390 $K = 400$ eigenvalues and eigenvectors are extracted to calculate the effective surface mass density according to Eq. (41). This was necessary in order to obtain accurate results for the effective surface mass density around the peak frequencies, because the peak frequencies also depend on the higher order modes, as apparent from Eq. (44).

395 The circular mass is placed at two different locations on the membrane to account for two different effects: In the first case, the mass is placed in the membrane center so that the mass exhibits only translational motion. In the second case, the mass is positioned with an offset of $\Delta x = 5 \text{ mm}$ from the membrane center to evoke rotational motion of the mass in addition to the
 400 translational motion.

For both mass positions, the CPU time of the proposed analytical model ($T_{\text{CPU}} \approx 115 \text{ s}$) was approximately 2.7 times lower than the CPU time of the

finite elements model calculations (not taking into account the time for pre- and post-processing of the numerical models). The memory usage of the analytical model (approx. 1000 MB) was 3 times higher than in the numerical simulations. This can be attributed to the implementation of the analytical model by the authors which has not been fully optimized in terms of memory usage.

The analytical and numerical results for the two mass positions are given in Fig. 6 with a comparison to the analytically obtained transmission loss of the bare membrane without the added mass. Both plots show that the analytical results are in excellent agreement with the results from the finite element model. Thus, the analytical model is capable to replicate the results obtained from a finite element discretization of a rectangular membrane metamaterial. In particular, the eigenfrequencies of the mass-loaded membrane which are found at the minima in the transmission loss curves are predicted correctly by the point matching approach. Likewise, the magnitude of the transmission loss obtained from the effective surface mass density is in excellent agreement with the numerical data, despite the acoustic wave length being in the order of magnitude of the membrane size at 1000 Hz.

As can be seen in Fig. 6, the transmission loss of the bare membrane is stiffness-controlled with a slope of -6 dB/octave, because the first eigenfrequency of the bare membrane $f_{m1} = 2510$ Hz is outside the considered frequency range. Compared to this, the transmission loss of the MAM is considerably larger around the peak frequencies, while at the resonance frequencies (especially the first one), the transmission loss is lower. Since these frequencies can be tuned by selecting suitable properties for the MAMs, so that the first resonance frequency occurs below and the peak frequencies inside the frequency range of interest, this shows the advantage of MAMs over the homogenous membrane for the low-frequency sound insulation.

The analytically obtained modeshapes of the first two symmetric eigenmodes for the centrally loaded rectangular membrane are shown in Fig. 7. The vibrational patterns of these eigenmodes correspond well to previous studies of the eigenmodes of MAMs [8, 17, 22]: The first eigenmode is characterized by large

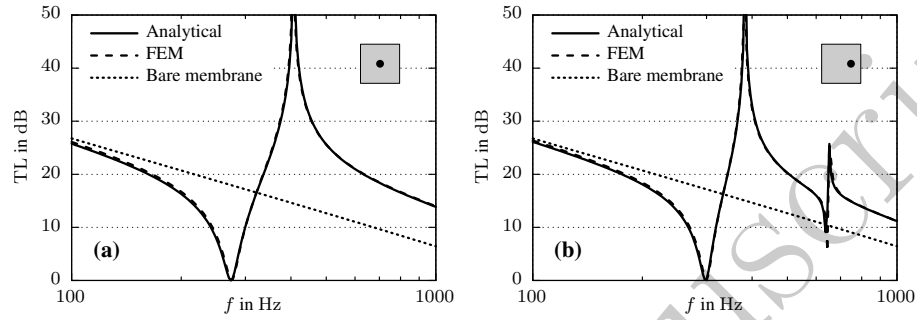


Figure 6: Comparison of the analytical and numerical results for the transmission loss of a rectangular membrane with a circular mass at two different locations. (a) Mass offset $\Delta x = 0$ mm; (b) $\Delta x = 5$ mm.

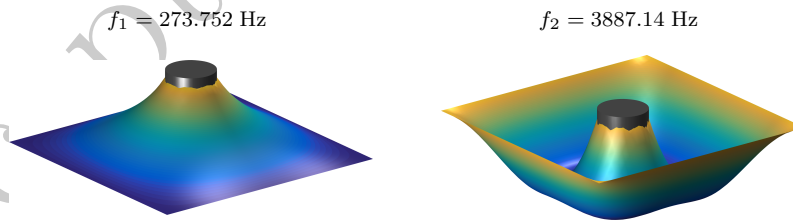


Figure 7: Analytically obtained mode shapes of the first (left) and second (right) symmetric eigenmode of the centrally loaded rectangular membrane.

vibration amplitudes of the central mass. Hence, this eigenmode is mainly de-
 435 termined by the added mass magnitude, the mass diameter, and the membrane
 properties. In the second modeshape, however, the vibration amplitude of the
 central mass is negligible, while the unloaded part of the membrane vibrates
 in-phase. Therefore, the added mass magnitude is not significant for the second
 eigenmode of the MAM [1, 8].

440 Finally, the non-dimensional effective surface mass density $\tilde{m}''/m''_{\text{tot}}$, where
 $m''_{\text{tot}} = m''_{\text{in}} + M/(L_x L_y)$ is the total surface mass density of the MAM, calculated
 using Eq. (41) for the case of the centrally loaded rectangular membrane is
 shown in Fig. 8. The effective surface mass density starts at negative infinity
 in the static limit ($f \rightarrow 0$). As discussed in [22], this can be explained by the
 445 fixed edges of the membrane which leads to a stiffness-dominated deflection at
 frequencies below the first eigenfrequency of the MAM. This deflection is in
 the same direction as the acting pressure difference and therefore, according to
 Eq. (35), \tilde{m}'' is negative. At the first eigenfrequency, the effective surface mass
 density is zero due to the resonance effect. Then, \tilde{m}'' becomes positive and
 450 quickly grows to values several orders of magnitude higher than m''_{tot} close to
 the first peak frequency. At f_{P1} , the effective surface mass density changes sign
 and approaches zero again at the second eigenfrequency. This behavior of the
 MAM's effective surface mass density, as predicted by the presented analytical
 model, compares well to the findings of previous theoretical and experimental
 455 studies [17, 22].

3.3. Circular membrane

For the circular membrane a radius of $R = 15$ mm is defined and the acoustic
 cavity length in the finite element model is set to $L_F = 2R$. The same element
 lengths as in the rectangular case are chosen and the analytical model is set-up
 460 with $N_r = N_\theta = 160$ modes in radial and azimuthal direction, respectively,
 which yields an overall number of modes of $N = 51040$. The coupling points
 and the number of extracted eigenpairs are the same as in the rectangular case.
 Also, two different mass locations are considered as well, with the circular mass

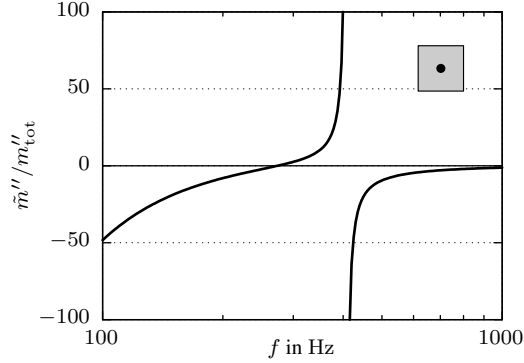


Figure 8: Non-dimensional effective surface mass density of the centrally loaded rectangular membrane.

placed in the membrane center and with a radial offset of $\Delta r = 5$ mm.

As for the rectangular membrane, the CPU time for the analytical calculation of the circular membrane ($T_{\text{CPU}} \approx 225$ s) was considerably lower than for the numerical simulation. In this case, the speed-up amounted to a factor of 3.8 due to the larger membrane area compared to the rectangular case which lead to a higher number of elements in the numerical model. Approximately 2000 MB of memory was used in the analytical calculations which, like in the rectangular case, was 3 times higher than in the numerical simulations.

Fig. 9 shows a comparison of the results obtained from the analytical model and the finite element model for both mass positions, as well as the transmission loss of the bare membrane. Like in the rectangular case, it is evident that the analytical results virtually match the numerical data and the eigenfrequencies of the mass-loaded membrane are predicted accurately. Hence, the analytical model yields satisfactory results for both rectangular and circular geometries. The comparison to the transmission loss of the bare membrane (first eigenfrequency $f_{m1} = 1811$ Hz) shows the same qualitative behavior that has been observed in § 3.2 for the rectangular membrane.

In Fig. 10 the analytically obtained vibrational patterns of the first two axisymmetric eigenmodes of the centrally loaded circular membrane are shown.

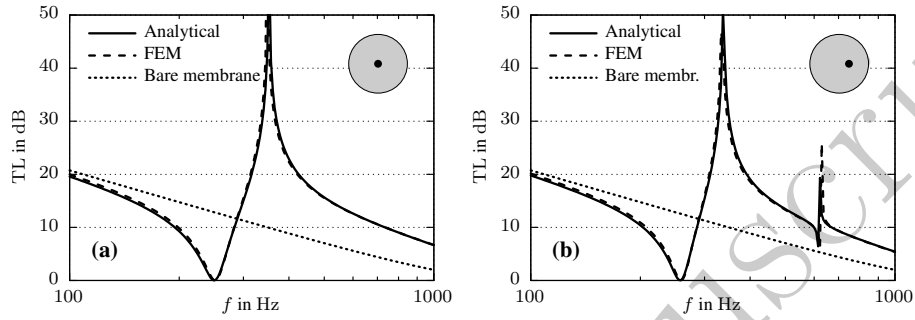


Figure 9: Comparison of the analytical and numerical results for the transmission loss of a circular membrane with a circular mass at two different locations. (a) Mass offset $\Delta r = 0$ mm; (b) $\Delta r = 5$ mm.

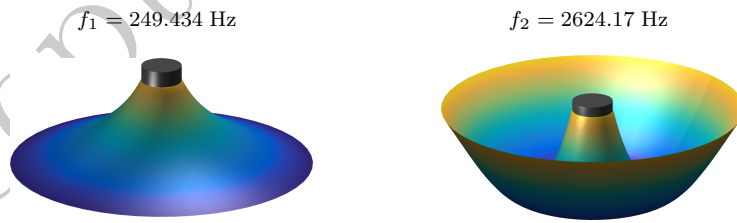


Figure 10: Analytically obtained mode shapes of the first (left) and second (right) axisymmetric eigenmode of the centrally loaded circular membrane.

These eigenmodes exhibit the same qualitative properties as the eigenmodes of the rectangular membrane shown in Fig. 7 with a strong vibration of the central mass in the first eigenmode and an annular-type vibration of the membrane with
 485 virtually fixed mass in the second eigenmode.

The analytically obtained non-dimensional effective surface mass density of the centrally loaded circular membrane, with $m''_{\text{tot}} = m''_{\text{m}} + M/(\pi R^2)$, is shown in Fig. 11. It shows the same qualitative behavior as already described in § 3.2
 490 for the case of the rectangular membrane.

3.4. Sensitivity of matching point spacing

One critical assumption during the derivation of the analytical model has been that the continuous membrane-mass interaction surface force γ'' can be sufficiently approximated by a finite set of point forces γ_i . In theory, the distributed point forces should converge to the unknown γ'' -distribution as the
 495 number of point forces I goes to infinity. For the application of the analytical model, however, it is more important to know, at which rate the point forces converge to the continuous distribution and how errors can be estimated for a given number of matching points. For this analysis, the first two eigenfrequencies f_1 and f_2 as well as the first peak frequency f_{P1} are calculated with
 500 the analytical model for the centrally loaded rectangular and circular membrane from the previous sub-sections. Four different coupling point spacings, $\Delta_\gamma = 1$ mm, 0.5 mm, 0.25 mm, and 0.125 mm, are considered and the Richardson extrapolation method is applied to estimate the order of convergence and the frequencies for the continuous case with $\Delta_\gamma \rightarrow 0$ [24].
 505

The order of convergence p is estimated from the results of the three finest coupling point spacings according to

$$p = \frac{\ln \frac{f^{(3)} - f^{(2)}}{f^{(2)} - f^{(1)}}}{\ln \kappa}, \quad (47)$$

where $f^{(1)}$ corresponds to a frequency calculated for the smallest point spacing $\Delta_\gamma^{(1)} = 0.125$ mm, $f^{(2)}$ is obtained for $\Delta_\gamma^{(2)} = 0.25$ mm, and $f^{(3)}$ for

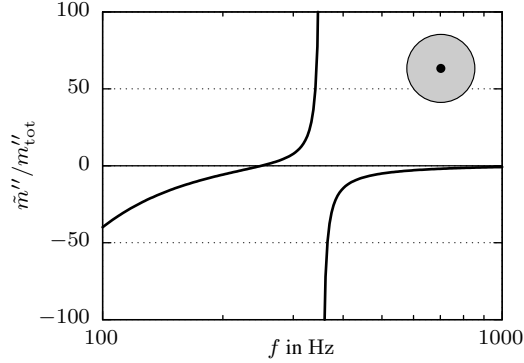


Figure 11: Non-dimensional effective surface mass density of the centrally loaded circular membrane.

510 $\Delta_\gamma^{(3)} = 0.5$ mm. κ is the refinement ratio (here: $\kappa = 2$): For a known order of convergence p , the extrapolated value \bar{f} for $\Delta_\gamma \rightarrow 0$ is estimated by

$$\bar{f} \approx f^{(1)} + \frac{f^{(1)} - f^{(2)}}{\kappa^p - 1}. \quad (48)$$

The analytically obtained and extrapolated frequencies are shown in Fig. 12 for the rectangular membrane and in Fig. 13 for the circular membrane, respectively. It can be seen that in both cases the first two natural frequencies and the first peak frequency converge asymptotically to finite values at $\Delta_\gamma = 0$ that are well predicted by the Richardson extrapolation. This indicates that the finite number of coupling point forces indeed converge to the continuous γ'' -distribution as the distance between the points approaches zero. Since the Richardson extrapolation is performed for the three finest point spacings, the extrapolated frequency curves in Figs. 12 and 13 match the analytical values for the three finest point spacings perfectly. Also, the natural frequencies f_1 and f_2 agree well with the extrapolated curve for the largest point spacing $\Delta_\gamma^{(4)} = 1$ mm which indicates that the natural frequencies already lie in the asymptotic range for the considered point spacings. The peak frequency f_{P1} , however, does not fall onto the extrapolated curve in both the rectangular and the circular membrane case when the largest point spacing is used. This im-

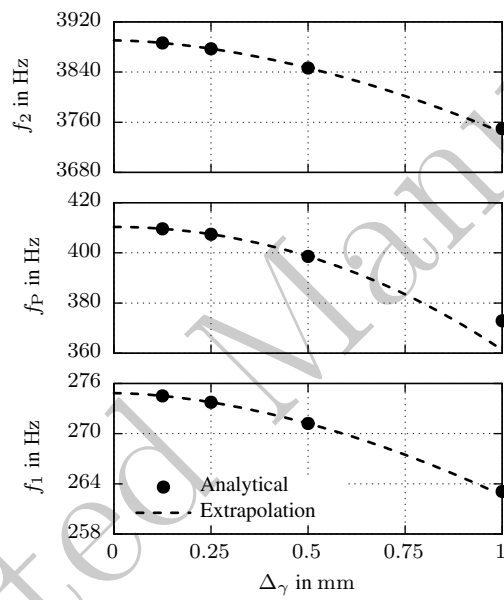


Figure 12: Analytical results for the first two natural frequencies and the first peak frequency of the centrally loaded rectangular membrane for different coupling point spacings Δ_γ . The dashed line shows estimated values from the Richard extrapolation.

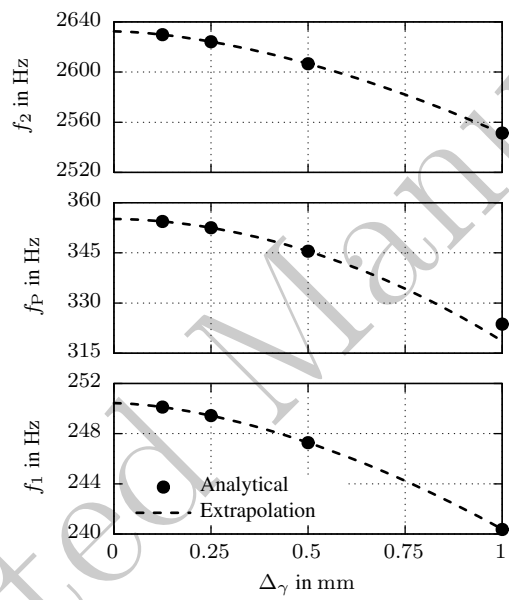


Figure 13: Analytical results for the first two natural frequencies and the first peak frequency of the centrally loaded circular membrane for different coupling point spacings Δ_γ . The dashed line shows estimated values from the Richard extrapolation.

plies that the asymptotic range of the peak frequencies starts at smaller point spacings than in the case of the natural frequencies. A possible explanation of this can be given by analyzing Eq. (44) which shows that the peak frequencies do not only depend on the dimensionless natural frequencies k_i , but also on the residuals A_i that are obtained from the eigenvectors which may have a different convergence behavior than the natural frequencies.

Additionally to the plots shown in Figs. 12 and 13, the corresponding numerical values and estimated orders of convergence are listed in Table 1. For the natural frequencies, the estimated order of convergence is $p \approx 1.7$ for the rectangular membrane and $p \approx 1.6$ for the circular membrane which shows that the rate of convergence of the natural frequencies is nearly independent of the membrane geometry. The peak frequency has a slightly higher order of convergence of $p \approx 2.0$ which confirms the difference in the convergence behavior between the natural and the peak frequencies, as observed in Figs. 12 and 13.

In order to estimate an error bound for the analytically predicted natural and peak frequencies, the grid convergence index (GCI), as proposed by Roache [25], is used. To calculate this error estimate, frequency results need to be obtained for a fine and a coarse point spacing ($f^{(f)}$ and $f^{(c)}$, respectively). Following the previous discussion on the convergence behavior, an order of convergence of $p = 1.6$ for the natural and peak frequencies likewise is a conservative choice. The grid convergence index is then calculated using

$$\text{GCI} = \frac{3}{\kappa^p - 1} \left| \frac{f^{(c)} - f^{(f)}}{f^{(f)}} \right|. \quad (49)$$

With Eq. (49), a frequency error estimate for the point spacing $\Delta_\gamma = 0.25$ mm that is chosen in the verification of the analytical model can be obtained. The resulting grid convergence indices lie in the range of $\text{GCI} \approx 1.0 \dots 1.5\%$ for the first two natural frequencies and $\text{GCI} \approx 3.0 \dots 3.2\%$ for the first peak frequency. As confirmed by the comparison to the finite element model results in the previous sub-sections, these error bounds are acceptable for an accurate prediction of natural and peak frequencies.

Table 1: Convergence of the first two natural frequencies and the first peak frequency of the centrally loaded rectangular and circular membrane with extrapolated values und estimated order of convergence.

I	Δ_γ (mm)	Rectangular membrane			Circular membrane		
		f_1 (Hz)	f_{P1} (Hz)	f_2 (Hz)	f_1 (Hz)	f_{P1} (Hz)	f_2 (Hz)
15	1.0	263.083	372.888	3749.63	240.360	323.671	2551.40
55	0.5	271.210	398.578	3846.50	247.280	345.472	2606.62
228	0.25	273.752	407.413	3887.14	249.434	352.488	2624.17
925	0.125	274.515	409.601	3886.39	250.115	354.391	2629.77
Extrapolated:		274.842	410.321	3890.39	250.430	355.099	2632.39
Order p :		1.736	2.014	1.728	1.661	1.882	1.648

4. Conclusions

In the first part of the present contribution an analytical model for the calculation of the low-frequency normal incidence transmission loss of mass-loaded rectangular and circular membranes was derived. A point matching approach was applied to couple the membranes with one or more rigid masses of arbitrary shape. The resulting linear eigenvalue problem was stated and the corresponding system matrices were presented for the rectangular and the circular membrane, respectively. Then, the effective surface mass density of the membrane was introduced to yield a simplified expression for calculating the low-frequency normal incidence transmission loss of the membrane. In the second part, the analytical model was verified with results from finite element model simulations which showed very good agreement between the predicted and the numerical data. A discussion on the sensitivity of the coupling point spacing showed that the discrete coupling point forces converge reasonably fast to the continuous force distribution between the membrane and the mass as the point spacing approaches zero. Finally, a method based upon the grid convergence index was presented to estimate an error bound on the predicted natural and

peak frequencies.

Due to the resulting linear eigenvalue problem, the presented analytical
575 model can be implemented with standard linear algebra methods. Since the in-
volved system matrices are generally sparse, efficient algorithms for the solution
of sparse generalized eigenproblems may be applied to calculate the eigenval-
ues and eigenvectors of the coupled system. Therefore, the presented analytical
model can be applied to the prototyping of numerical or experimental models
580 involving MAMs or automated optimizations of mass-loaded membranes, where
computational efficiency is crucial. Since the concept of the effective surface
mass density is only valid for acoustic wavelengths larger than the membrane
itself, the proposed method for the calculation of the normal incidence trans-
mission loss is confined to low frequencies. However, this can be extended to
585 arbitrary frequencies, e.g. by employing the method shown in [17] to the calcu-
lated eigenvalues and -vectors, which, nevertheless, requires the application of
numerical integration.

For an industrial application of the discussed MAMs in large-scale struc-
tures, it is necessary to consider the rather small membrane-metamaterials as
590 periodically arranged unit cells of a larger structure. In [10, 26] it is shown that
the desired transmission loss behavior of MAMs basically extrapolates to larger
structures with multiple MAM unit cells. The global resonance behavior and
imperfect boundary conditions of large-scale structures, however, may affect the
transmission loss negatively. Also, the influence of oblique and diffuse incident
595 sound fields needs to be considered for such structures. It was demonstrated in
[11] that the qualitative behavior of absorbent MAMs is very similar for oblique
incidence angles up to 60° . For a better understanding of this effect, the pre-
sented model, which considers normal incident plane acoustic waves only, can be
modified accordingly to enable the calculation of oblique and diffuse incidence
600 transmission losses.

Acknowledgements

This work has been performed under the framework of the LuFo IV-4 project Comfortable Cabin for Low-Emission Aircraft (COCLEA), funded by the Federal Ministry for Economic Affairs and Energy (grant number: 20K1102D). The
605 financial support is gratefully acknowledged by the authors.

- [1] Z. Yang, J. Mei, M. Yang, N. H. Chan, P. Sheng, Membrane-type acoustic metamaterial with negative dynamic mass, *Physical Review Letters* 101 (2008) 204301.
- [2] Z. Liu, X. Zhang, Y. Mao, Y. Y. Zhu, Z. Yang, C. T. Chan, P. Sheng,
610 Locally resonant sonic materials, *Science* 289 (2000) 1734–1736.
- [3] K. M. Ho, Z. Yang, X. X. Zhang, P. Sheng, Measurements of sound transmission through panels of locally resonant materials between impedance tubes, *Applied Acoustics* 66 (2005) 751–765.
- [4] N. Fang, D. Xi, J. Xu, M. Ambati, W. Srituravanich, C. Sun, X. Zhang,
615 Ultrasonic metamaterials with negative modulus, *Nature Materials* 5 (2006) 452–456.
- [5] S. H. Lee, C. M. Park, Y. M. Seo, Z. G. Wang, C. K. Kim, Acoustic metamaterial with negative modulus., *Journal of Physics: Condensed Matter* 21 (2009) 175704.
- 620 [6] S. H. Lee, C. M. Park, Y. M. Seo, Z. G. Wang, C. K. Kim, Composite acoustic medium with simultaneously negative density and modulus, *Physical Review Letters* 104 (2010) 054301.
- [7] Z. Yang, H. M. Dai, N. H. Chan, G. C. Ma, P. Sheng, Acoustic metamaterial panels for sound attenuation in the 50–1000 Hz regime, *Applied Physics Letters* 96 (2010) 041906.
625
- [8] C. J. Naify, C.-M. Chang, G. McKnight, S. Nutt, Transmission loss and dynamic response of membrane-type locally resonant acoustic metamaterials, *Journal of Applied Physics* 108 (2010) 114905.

- [9] Y. Zhang, J. Wen, Y. Xiao, X. Wen, J. Wang, Theoretical investigation of
630 the sound attenuation of membrane-type acoustic metamaterials, *Physics Letters A* 376 (2012) 1489–1494.
- [10] C. J. Naify, C.-M. Chang, G. McKnight, S. R. Nutt, Scaling of membrane-type locally resonant acoustic metamaterial arrays, *The Journal of the Acoustical Society of America* 132 (2012) 2784–92.
- [11] J. Mei, G. Ma, M. Yang, Z. Yang, W. Wen, P. Sheng, Dark acoustic
635 metamaterials as super absorbers for low-frequency sound, *Nature Communications* 3 (2012) 756.
- [12] G. Ma, J. Mei, M. Yang, Z. Yang, W. Wen, P. Sheng, Low-frequency total absorption with membrane-type acoustic metamaterial, in: *Proceedings of the 19th ICSV, Vilnius, Lithuania, 2012.*
640
- [13] E. T. Kornhauser, D. Mintzer, On the vibration of mass-ãloaded membranes, *The Journal of the Acoustical Society of America* 25 (1953) 903–906.
- [14] H. Cohen, G. Handelman, On the vibration of a circular membrane with
645 added mass, *The Journal of the Acoustical Society of America* 29 (1957) 229–233.
- [15] C. Y. Wang, Vibration of an annular membrane attached to a free, rigid core, *Journal of Sound and Vibration* 260 (2003) 776–782.
- [16] H. Tian, X. Wang, Y.-H. Zhou, Theoretical model and analytical approach
650 for a circular membrane-ring structure of locally resonant acoustic metamaterial, *Applied Physics A* 114 (2013) 985–990.
- [17] Y. Chen, G. Huang, X. Zhou, G. Hu, C.-T. Sun, Analytical coupled vibroacoustic modeling of membrane-type acoustic metamaterials: Membrane model, *The Journal of the Acoustical Society of America* 136 (2014)
655 969–979.

- [18] A. W. Leissa, Vibration of plates, NASA SP-160, 1969.
- [19] Y. Saad, Numerical methods for large eigenvalue problems, 2nd ed., Society for Industrial and Applied Mathematics, Philadelphia, 2011.
- [20] F. J. Fahy, P. Gardonio, Sound and structural vibration: radiation, transmission and response, Academic press, Oxford, UK, 2007.
- [21] M. Yang, G. Ma, Z. Yang, P. Sheng, Coupled membranes with doubly negative mass density and bulk modulus, *Physical Review Letters* 110 (2013) 134301.
- [22] M. Yang, G. Ma, Y. Wu, Z. Yang, P. Sheng, Homogenization scheme for acoustic metamaterials, *Physical Review. B* 89 (2014) 064309.
- [23] W. Soedel, Vibrations of shells and plates, 3rd ed., Marcel Dekker, Inc., New York, 2004.
- [24] W. L. Oberkampf, C. J. Roy, Verification and validation in scientific computing, volume 5, Cambridge University Press, Cambridge, 2010.
- [25] P. J. Roache, Perspective: a method for uniform reporting of grid refinement studies, *Journal of Fluids Engineering* 116 (1994) 405–413.
- [26] C. J. Naify, C.-M. Chang, G. McKnight, F. Scheulen, S. Nutt, Membrane-type metamaterials: Transmission loss of multi-celled arrays, *Journal of Applied Physics* 109 (2011) 104902.